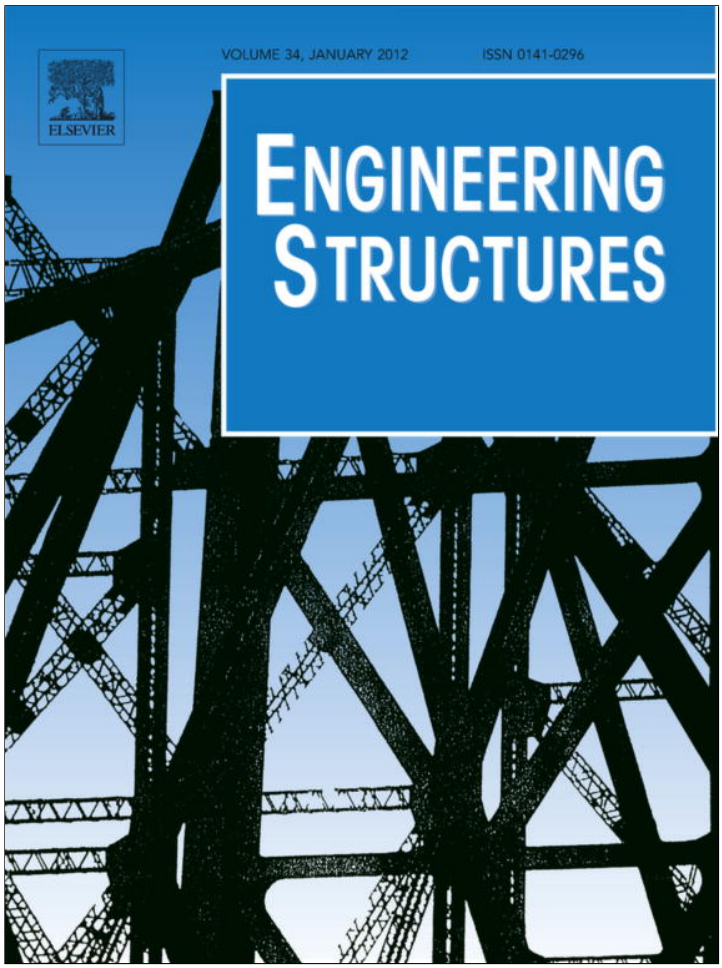

(This is a sample cover image for this issue. The actual cover is not yet available at this time.)

Engineering Structures 37 (2012) 214–223

Contents lists available at SciVerse ScienceDirect

Engineering Structures

journal homepage: www.elsevier.com/locate/engstruct

Linkage-based movable bridges: Design methodology and three novel forms ☆

A.P. Thrall [a,*,1], S. Adriaenssens [b], I. Paya-Zaforteza [c], T.P. Zoli [d]

[a] Department of Civil and Environmental Engineering, Princeton University, Engineering Quadrangle E321, Princeton, NJ 08544, USA
[b] Department of Civil and Environmental Engineering, Princeton University, Engineering Quadrangle E332, Princeton, NJ 08544, USA
[c] Departamento de Ingeniería de la Construcción y Proyectos de Ingeniería Civil ICITECH, Universidad Politécnica de Valencia, Valencia, Spain
[d] HNTB Corporation, 5 Penn Plaza, 5th Floor, New York, NY 10001, USA

ARTICLE INFO

Article history:
Received 1 August 2011
Revised 9 December 2011
Accepted 17 December 2011

Keywords:
Movable bridge
Linkage
Structural optimization
Descent local search
Multi-objective simulated annealing

ABSTRACT

Linkages have been widely used in machines and deployable structures, but these mechanisms have rarely been employed in the design of movable bridges. This paper explores the use of linkages both to actuate the kinematic motion and to serve as structural elements of movable bridges. First, the design methodology for these forms is presented which includes (1) physical shape-finding to develop a conceptual design, (2) generation of a parametric model and kinematic equations, and (3) multi-objective structural optimization for minimum self-weight and minimum force for operation. This optimization procedure includes shape optimization to determine the lengths and relative angles of members and sizing optimization to design the section profiles of members to meet the specifications of current American bridge design code. Heuristic algorithms, including descent local search and multi-objective simulated annealing, are employed. Three novel linkage-based forms, featuring 38 m movable spans, that were designed using this methodology are presented. This research suggests the beginning of an investigation into alternative forms for movable bridges using linkages.

1. Introduction and motivation

Designers of movable bridges over the last century have primarily utilized standard bascule, swing, and vertical lift forms [1,2]. Today there are 1900 operational, movable bridges in the United States, including 770 bascules, 750 swing, 270 vertical lift, and 110 other miscellaneous types [2]. Bascule bridges are the most common type being constructed today, comprising 65% of new movable bridge construction over the last two decades [2]. Linkages – a type of mechanism which is an assembly of one-dimensional, rigid bars connected by lower-order pairs (revolute, prismatic, screw, cylindric, spherical, or planar connections) – have widely been used in the development of machines since the 18th century and in deployable structures since Emilio Perez Piñero's 1961 traveling theater [3–5]. However, there has been limited employment of linkages in the field of movable bridge design. This paper explores the application of linkages to actuate the motion of movable bridges while also serving structural purposes. Such structures will be referred to as linkage-based movable bridges.

The formal study of mechanisms dates back to the 18th century when Leonhard Euler (1707–1783) introduced full kinematic study and analysis in "Mechanica, sive, Motus scientia analytice exposita" (mechanics, or the science of motion expounded analytically) [3,6]. Around the same time (1784), James Watt (1736–1819) explored the coupler-point motion of the four-bar linkage and applied this new range of motion in his double-acting steam engine [3]. From these early studies and applications, a wealth of research developed in the field of kinematics which underwent its greatest period of development through the end of the 19th century [3]. During this height of interest in complex mechanisms, there was a great interest in developing new forms for bascule, vertical lift, and retractile movable bridges using this technology. However, these new forms employed complicated roller bearings and locking mechanisms that required constant maintenance. As a result, many of these new forms fell out of use and simple designs which minimized the number of moving parts became the trend [2]. One of the few successful implementations of mechanisms in movable bridge design are the heel trunnion designs developed by Joseph Strauss (1870–1938). Fig. 1 shows a four-bar linkage in a Strauss heel trunnion bascule (connecting nodes T, E, H, and F). Trunnions at Point E (supported by a pier) and Point T (supported by a counterweight tower) remain at the same location. An operating pinion moves along rack S, thereby decreasing the distance between C and H. As distance CH decreases, the counterweight and the deck rotate counterclockwise [7]. The linkage here is utilized only for moving the counterweight (W) and its members do not

☆ This document is a collaborative effort.

* Corresponding author. Tel.: +15746312533.
E-mail addresses: athrall@nd.edu (A.P. Thrall), sadriaen@princeton.edu (S. Adriaenssens), igpaza@upvnet.upv.es (I. Payá-Zaforteza), tzoli@hntb.com (T.P. Zoli).
[1] Present address: Department of Civil Engineering and Geological Sciences, University of Notre Dame, 159 Fitzpatrick Hall, Notre Dame, IN 46556, USA.

0141-0296/$ - see front matter © 2011 Elsevier Ltd. All rights reserved.
doi:10.1016/j.engstruct.2011.12.031

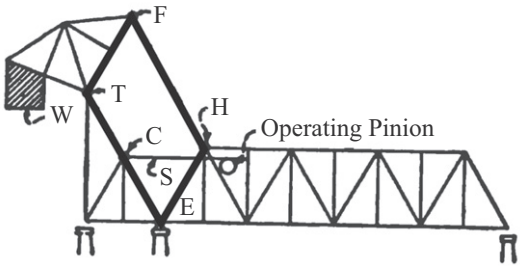

Fig. 1. Elevation of the Strauss Heel-trunnion Bascule. The four-bar linkage is shown in bold lines. Image courtesy of Waddell (1916) with alterations by the authors.

act as structural members to support the deck. Though Strauss's design does not realize linkages as both structural and kinematic elements, it shows that simple linkage systems (e.g. four-bar linkages) are capable of being successfully employed and maintained in movable bridge design. Advances in technology today have made innovations in the actuation of movable bridges increasingly feasible. Design firms have taken advantage of advances in the field of hydraulics to integrate structure and kinematics for the first time. Examples include the piston-stayed bridges by Ney and Partners (e.g. Tervate and Temse Bridges in Belgium) and the Humpback Bridge by Schlaich Bergermann and Partners [8–10]. These design firms have integrated structure and kinematics for the first time, resulting in elegant and efficient forms that employ these advances in technology. Given these new opportunities, this paper suggests the beginning of an exploration of designing alternative forms for movable bridges using linkages.

This paper first presents a design methodology and optimization procedure for linkage-based movable bridges, including (1) physical-shape finding, (2) parametric modeling and generating kinematic equations, and (3) multi-objective structural optimization for minimum self-weight and minimum force for operation. Then, three novel 38 m span linkage-based forms are presented which meet the design requirements for the movable section of the Woodrow Wilson Bridge Design Competition (November 1998) for the crossing between Alexandria, Virginia and Oxon Hill, Maryland, USA [11]. Finally, the paper concludes with a discussion of the rich opportunities for further exploration of linkage-based movable bridge forms.

2. Design methodology and optimization procedure

This paper proposes a methodology for the design and optimization of linkage-based movable bridge forms. First, a physical shape-finding process is employed to develop a conceptual design. To determine the geometry (meaning the lengths and relative angles for each member) and the section profiles of each of the members of a design concept, multi-objective structural optimization for minimum self-weight and minimum force for operation is employed. The required input for this procedure includes a parametric model which defines the initial geometry based on a few parameters. Kinematic equations which can calculate the coordinates of each node as a function of these parameters and the angle of opening are also required. The result of the optimization process is a pareto-optimal set of solutions from which an engineer can choose a final solution based on design priorities.

The following sub-sections will detail this procedure, employing one form presented in this paper for demonstration.

2.1. Physical shape-finding

The conceptual design of each of the proposed forms was developed through shape-finding using physical models. This research focused on the utilization of linkages as the main kinematic element of movable bridges, specifically investigating the four-bar linkage – a linkage comprised of four rigid bars connected by four revolute lower pair connectors (connections that permit rotation but no relative translation) [3]. To gain an intuition into potential kinematics, planar, physical models of four-bar linkages were built using K'NEX toys (left image of Fig. 2) [12]. In the physical model shown in Fig. 2, members connecting nodes 1–2, 1–4, 2–3, and 3–4 are the four, fixed-length bars of the linkage which are pin-connected at either end to permit rotation. Nodes 1 and 2 are pin supported (restrained displacement, free rotation). By "driving" node 4, node 3 follows. Node 3 and 4 each sweep arcs of different radii (based on their respective lengths).

With this physical model, the engineer can develop a conceptual design by envisioning the potential kinematic motion. First, the structural supports of the linkage, such as the pin supports at nodes 1 and 2 in Fig. 2, need to be selected so that the mechanism is sufficiently kinematically constrained. The engineer should then consider the manner in which a deck can be attached to the linkage to minimize bending in the deck, thereby potentially facilitating a lighter deck design. An actuation system must be devised which rotates the linkage and lifts the deck. Potential options include an operating rope with a conventional gear driven mechanical system or a piston. With such basic definitions of the system, it can then be evaluated from a structural standpoint. More specifically, the engineer should consider which members would be under compression or tension under their own self-weight, the self-weight of the deck, wind load on the deck (when the structure is moving and fully open) and live load on the deck (when the structure is closed). These loads are particularly important to consider since they are typically the worst loadings for bascule bridges [8]. It is advisable to select linkages that do not require long compression members due to their reduced capacity from buckling. This is particularly important when considering the linkage in the configuration in which the structure would be closed since additional live load could dramatically increase axial loads on linkage members. It is also important to consider the use of cables, keeping in mind that these elements would need to remain in tension throughout movement. With these considerations, an engineer can make informed decisions regarding the conceptual design.

The physical model shown in the left of Fig. 2 was utilized to develop the conceptual design for a movable bridge form, called the back-stay bascule design, shown on the right. Node 1 corresponds to point A, node 2 corresponds to point B, node 3 corresponds to point E, and node 4 corresponds to point D. Member BC is the deck which is shown as closed. The linkage is highlighted by dashed lines. Three supports (points F, A, and B) are idealized as pin supports. There is no connection between members AD and BE. Pin connections are indicated in the diagram as filled circles. Member DG is a fixed length rope that connects the linkage to the deck. Actuation is performed through member EF which is a variable length element. For the purpose of this research, this member is assumed to be an operating rope with a conventional gear driven mechanical system at point F and is required to always be in tension. Alternatively, this requirement could be released and a piston could be utilized instead. Regardless of the choice of mechanical system, as the variable length element shortens, the deck is lifted. An additional live load rope connecting points E and F carries the live load of the bridge when it is closed, but goes slack as the variable length element EF shortens and lifts the deck.

This physical shape-finding process was utilized to determine the form of a particular design. In a traditional approach to structural design, once an engineer has developed a conceptual design, the next step would involve selecting the geometry and section profiles. Different geometric selections using the same form could result in very different designs. To fully explore this form, an

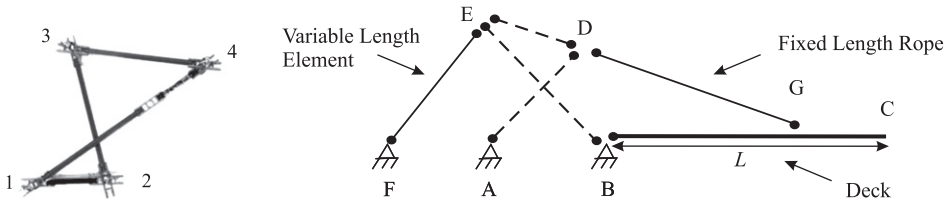

Fig. 2. Physical model (left) and conceptual design in the closed position (right). The different shades of bars in the model simply denote the different sizes of bars. The bar connecting nodes 1 and 4 includes a link that joins two different length bars.

engineer would need to consider a variety of geometries and design section profiles for each. It is obvious that this would be a lengthy trial-and-error process. Alternatively, this paper proposes a structural optimization procedure that can explore a wide range of geometries quickly to determine an optimized solution. The input required for this optimization includes a parametric model and kinematic equations that describe the motion of the system. This will be discussed in the following sub-section.

2.2. Parametric model and kinematic equations

For each design, a two-dimensional, parametric model of the system was developed so that a few geometric parameters define the lengths and relative angles of all members. For example, for the conceptual design in Fig. 2, these parameters include the initial coordinates of points A, B, E, and D relative to point F ($X_{Ao}, X_{Bo}, X_{Eo}, Y_{Eo}, X_{Do}$, and Y_{Do}; where X refers to the horizontal coordinate, Y to the vertical coordinate, and o indicates the initial position). A system of kinematic equations can then be utilized to compute the coordinates of all nodes as a function of the angle of opening β and these geometric parameters. The kinematic equations for the design concept in Fig. 2 are given in the following paragraph.

Point F is a pin support which remains fixed at the origin. Likewise, the other pin supports at points A and B remain fixed with coordinates: $X_A = X_{Ao}, Y_A = 0$ and $X_B = X_{Bo}, Y_B = 0$, respectively. Point C is calculated by:

$$X_C = X_{Bo} + L \cdot \cos\beta \tag{1}$$

$$Y_C = L \cdot \sin\beta \tag{2}$$

where L is the length of the deck. Point G (where the fixed length rope picks up the deck) was selected to make the bending moment along the deck as even as possible under a uniform load (q) in the closed position ($\beta = 0$). This loading and position were selected since the closed bridge under combined dead and live load would be the most critical position for bending in the deck. If the deck is idealized as a pin support at point B and a roller represents the support of the rope DG, then an approximate bending moment diagram for the deck is represented in Fig. 3. To achieve a more uniform bending moment along the deck, the length (l_{BG}) was selected so that the magnitudes of the maximum negative and positive bending moments are equal. The magnitude of the maximum negative bending moment (M_-, shown between points B and G) is given by:

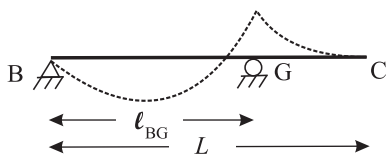

Fig. 3. Idealized Deck with superimposed bending moment (dashed).

$$M_- = \frac{q}{2}\left\{L - \frac{L^2}{2l_{BG}}\right\}^2 \tag{3}$$

and the magnitude of the maximum positive bending moment (M_+ at point G) is given by:

$$M_+ = \frac{q}{2}\{L - l_{BG}\}^2 \tag{4}$$

Here, a negative moment refers to compression on top and a positive moment refers to tension on top. Setting these expressions equal, the length l_{BG} can be expressed in terms of the full span length (L) as $l_{BG} = \frac{\sqrt{2}L}{2}$. The coordinates of G as a function of the angle of opening can then be calculated as:

$$X_G = X_{Bo} + l_{BG} \cdot \cos\beta \tag{5}$$

$$Y_G = l_{BG} \cdot \sin\beta \tag{6}$$

To calculate the coordinates points D and E, several lengths need to be calculated as follows. The distance between pin supports A and B (l_{AB}), is $l_{AB} = X_{Bo} - X_{Ao}$. The fixed length of member AD (l_{AD}) can be calculated using the Pythagorean theorem as follows:

$$l_{AD} = \sqrt{(X_{Ao} - X_{Do})^2 + (Y_{Ao} - Y_{Do})^2} \tag{7}$$

The fixed length of rope DG (l_{DG}) can be calculated using the Pythagorean theorem as follows:

$$l_{DG} = \sqrt{(X_{Go} - X_{Do})^2 + (Y_{Go} - Y_{Do})^2} \tag{8}$$

The distance between points A and G (l_{AG}) changes as a function of the angle β and is calculated at each stage of opening using the Pythagorean theorem as follows:

$$l_{AG} = \sqrt{(X_A - X_G)^2 + (Y_A - Y_G)^2} \tag{9}$$

Then the coordinates of D are calculated as follows:

$$X_D = X_A + l_{AD}\cos\left\{\arccos\frac{l_{AB}^2 + l_{AG}^2 - l_{BG}^2}{2l_{AB}l_{AG}} + \arccos\frac{l_{AD}^2 + l_{AG}^2 - l_{DG}^2}{2l_{AB}l_{AG}}\right\} \tag{10}$$

$$Y_D = l_{AD}\sin\left\{\arccos\frac{l_{AB}^2 + l_{AG}^2 - l_{BG}^2}{2l_{AB}l_{AG}} + \arccos\frac{l_{AD}^2 + l_{AG}^2 - l_{DG}^2}{2l_{AB}l_{AG}}\right\} \tag{11}$$

To calculate the coordinates of point E, it is necessary to determine the lengths of members EB and ED (l_{EB} and l_{ED}, respectively) using the Pythagorean theorem as follows:

$$l_{EB} = \sqrt{(X_{Eo} - X_{Bo})^2 + (Y_{Eo} - Y_{Bo})^2} \tag{12}$$

$$l_{ED} = \sqrt{(X_{Eo} - X_{Do})^2 + (Y_{Eo} - Y_{Do})^2} \tag{13}$$

The distance between points B and D (l_{BD}) changes with the angle β and can be calculated by:

$$l_{BD} = \sqrt{(X_D - X_B)^2 + (Y_D - Y_B)^2} \tag{14}$$

Then the coordinates of E are calculated by:

$$X_E = X_B + l_{EB}\cos\left\{\beta + \arccos\frac{l_{BG}^2 + l_{BD}^2 - l_{DG}^2}{2l_{BG}l_{BD}} + \arccos\frac{l_{EB}^2 + l_{BD}^2 - l_{ED}^2}{2l_{EB}l_{BD}}\right\} \quad (15)$$

$$Y_D = l_{EB}\sin\left\{\beta + \arccos\frac{l_{BG}^2 + l_{BD}^2 - l_{DG}^2}{2l_{BG}l_{BD}} + \arccos\frac{l_{EB}^2 + l_{BD}^2 - l_{ED}^2}{2l_{EB}l_{BD}}\right\} \quad (16)$$

Using these equations, one can find the coordinates of all nodes as a function of the angle of opening β given the initial coordinates of A, B, E, and D relative to point F. Note that this section has presented only the equations for the first of the three forms presented in this paper (the back-stay bascule design). The reader is referred to Thrall (2011) for the equations for the other two forms [13].

2.3. Shape and sizing structural optimization

The geometry (meaning the lengths and relative angles of members) is determined through multi-objective shape optimization for minimum self-weight and minimum force for operation using multi-objective simulated annealing (MOSA). The section profiles of the steel, linkage elements are selected from a database of industry standards using a nested sizing optimization routine for minimum self-weight using the descent local search (DLS) algorithm. Fig. 4 provides a flow-chart of the optimization procedure. The following sub-sections provide formal problem definitions and detailed descriptions of the algorithms employed.

2.3.1. Problem definitions

The shape optimization is defined as:

$$\begin{aligned} \underset{\mathbf{g}}{\text{minimize}} \quad & W(\mathbf{g},\mathbf{s}) = \textstyle\sum_{i=1}^{nel} \rho A_i(\mathbf{s}) L_i(\mathbf{g}) \\ & P(\mathbf{g},\mathbf{s}) = \max(N_1, N_2, \ldots, N_t) \\ \text{such that} \quad & q_k(\mathbf{g}) \leqslant 0 \quad k = 1, \ldots, R. \end{aligned} \quad (17)$$

where **g** refers to the geometric design variables – the geometric parameters in the parametric model which define the length L and the relative angle of each member – and **s** refers to the sizing design variables – the section profiles of linkage elements selected from a database of industry standards which identifies the area (A), moment of inertia, etc. Multi-objective shape optimization for minimum self-weight (W) and minimum force for operation (P) is employed to determine an optimized set of geometric design variables **g**. Nested sizing optimization determines the sizing design variables **s** for each geometry. However, both objective functions depend on both the geometric and sizing design variables. The minimum self-weight objective function (W), chosen to minimize the amount of material used, is defined as the summation over *nel* number of members of the density (ρ) times the product of the area and length of each member. The minimum force for operation objective function (P) is defined as the maximum force in the operating member

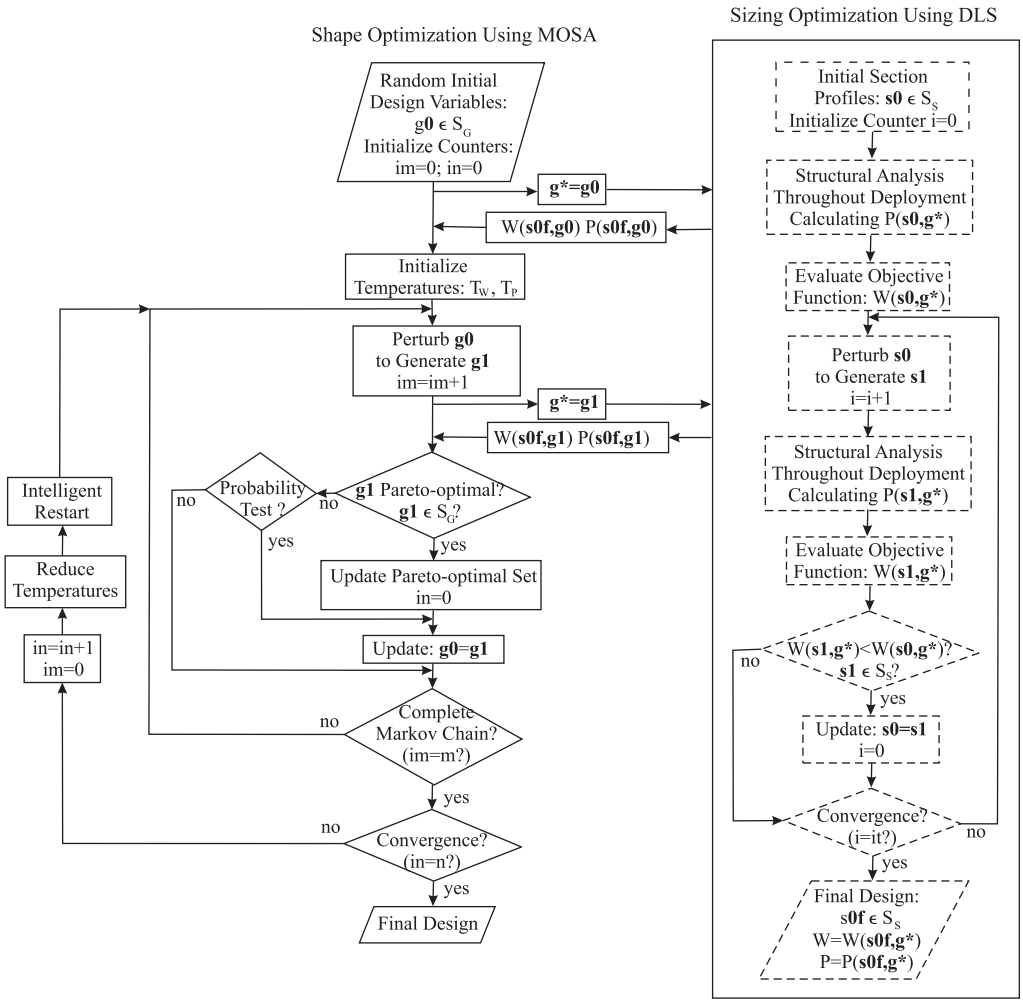

Fig. 4. Flow chart of structural optimization process.

(N) during all stages of opening (denoted by the index t). The force in the operating member was chosen as a second objective function since it is related to the power required for operation. The constraint equations q refer to the R number of problem-specific constraints that sufficiently confine the system to open with the appropriate kinematics.

For each geometry considered, the linkage members (the reader is referred to Section 3 for a discussion of the deck and rope design) were selected from a database of API line pipe [14] using nested sizing optimization, defined as:

$$\begin{aligned} &\underset{\mathbf{s}}{\text{minimize}} \quad W(\mathbf{g},\mathbf{s}) = \sum_{i=1}^{nel} \rho A_i(\mathbf{s}) L_i(\mathbf{g}) \\ &\text{such that} \quad c_j(\mathbf{g},\mathbf{s}) \leqslant 0 \quad j = 1,\ldots,M. \end{aligned} \tag{18}$$

where the constraints (c) refer to the requirement that each member meet the American Association of State Highway and Transportation Officials (AASHTO) Load and Resistance Factor Design (LRFD) Bridge Design Specifications throughout opening. The M number of equations refer to constraints for axial strength, slenderness, local buckling, bending, shear, and combined axial load and bending under factored load combinations [15]. Alternative design codes could easily be implemented as constraints instead. To check these constraints, a first-order elastic structural analysis is performed when the bridge is in the closed position and as the bridge opens at every 10 degree increment. Note that during this nested profile optimization procedure, the shape of the system (meaning the geometric design variables) is held constant. To analyze the bridge at each stage of opening, the positions of nodes are calculated using the kinematic equations (developed for each form), values for the geometric design variables, and the angle of opening. Only strength limit states are currently considered. For the purpose of this research, dead load, live load (distributed lane load only), and wind load (applied longitudinally against the deck) are considered using AASHTO LRFD Bridge Design Specifications Load Combination Strength I (1.25 dead load + 1.75 live load) in the closed position and AASHTO LRFD Movable Highway Bridge Design Specifications 2007 Strength BV II (1.25 dead load + 1.25 wind load) in the open positions [15,16].

This methodology aids the design of movable bridges at the sketch design phase. Generally, the worst loading combination considered during preliminary design of bascule bridges occurs under self-weight and wind load on the deck while opening [8]. In a traditional evaluation approach all phases of opening are individually analyzed for these loading conditions and the worst analysis results are designed for. The presented approach allows the structure to be optimized while all opening phases are evaluated. Once the overall geometry and initial shape sizing is established through this method that reduces operating force and self-weight, a full engineering analysis has to be carried out. The final system has to be designed and detailed according to prevalent codes to cope with additional loads and limit states (e.g. fatigue and fracture, extreme event). Serviceability limit states in AASHTO design code, including optional deflection limitations on the bridge deck, should be considered in the final design. Dead load deflections could also be avoided by introducing camber in the final design.

2.3.2. Optimization algorithms

Since these problems are non-convex, nonlinear, and contain discrete conditions, heuristic algorithms were selected to search the feasible design space for optimized solutions. Fig. 4 shows a flow chart of the optimization procedure. Shape optimization, shown in solid lines on the left of Fig. 4, employed a multi-objective simulated annealing (MOSA) algorithm. The nested sizing optimization, shown in dashed lines on the right of Fig. 4, is performed using the descent local search (DLS) algorithm. The effectiveness of single objective shape and sizing optimization of deployable structures using this strategy has previously been demonstrated by an author [17]. The following paragraphs describe these algorithms.

Shape optimization is performed using a multi-objective version of the simulated annealing (SA) algorithm. This heuristic algorithm, first proposed by Kirkpatrick et al. [18], searches the feasible design space based on an analogy to crystal formation when a high temperature mass is slowly cooled. During this physical process, the energy of the system generally decreases. However, there is a certain probability (Pr) that higher energy configurations can occur which ultimately permit the mass to reach a lower energy configuration. This probability is given by $Pr = \exp(-\Delta E/T)$, where ΔE refers to the difference in energy between the configurations and T refers to the temperature. When the temperature is lowered, this probability decreases thereby permitting fewer high energy configuration to occur. Kirkpatrick et al. [18] proposed an iterative improvement optimization algorithm based on an analogy to this physical process, where the energy is related to the objective function. The probability (Pr) then relates to a probability of accepting higher value objective function solutions, where T is a parameter that can be controlled by the user. This probability enables the algorithm to escape a local minimum. The algorithm begins with a high value of T which permits more higher value solutions to be considered. The temperature is slowly reduced as the algorithm progresses, thereby reducing the probability of exploring higher value solutions [18]. To consider several objective functions simultaneously, Suppapitnarm et al. [19] proposed a multi-objective approach to SA. Traditionally, multi-objective approaches involve generating one objective function that is a weighted combination of all functions to be considered. Suppapitnarm et al. [19] instead advocate evaluating all objective functions for each set of design variables. At each stage of evaluation, a pareto-optimal set of solutions is formed, where a pareto-optimal solution is a solution which is not overshadowed by any other solution [19]. The engineer can select a final solution from the final pareto-optimal set based on design priorities. SA and MOSA have been previously employed for structural optimization (see ex. [20–24]). The following paragraph will more specifically describe how MOSA was implemented for this problem.

The version of MOSA employed for shape optimization in this research (Fig. 4, solid lines) begins by randomly selecting an initial, feasible set of geometric design variables ($\mathbf{g0}$) from a discrete database of lengths. A solution is deemed feasible if it meets all geometric constraints throughout opening ($\mathbf{g0}$ is an element of S_G, where S_G is the set of all feasible solutions). Sizing optimization (described in the following paragraph, shown in dashed lines in Fig. 4) is then employed to determine an optimal set of section profiles for that specific geometry. During this process, both of the objective functions are evaluated and returned to the shape optimization loop ($W(\mathbf{s0f},\mathbf{g0})$, $P(\mathbf{s0f},\mathbf{g0})$, where $\mathbf{s0f}$ refers to the final selection for section profile variables from the sizing optimization process). With an initial, feasible geometry selected, an initial pareto-optimal set is defined [19]. Temperatures for both the weight and force objective functions (T_W and T_P, respectively) are initiated as values that accept between 20% and 40% of high value objective function solutions [25]. The MOSA algorithm then begins to search the feasible design space by updating this pareto-optimal set. A new solution ($\mathbf{g1}$) is found by randomly perturbing the geometric design variables in $\mathbf{g0}$. With this new solution, sizing optimization is again performed for that geometry. The pareto-optimal solution is then updated. If $\mathbf{g1}$ is pareto-optimal, then it becomes the new working solution ($\mathbf{g0}$) upon which the algorithm iterates. If not, the algorithm calculates the probability of keeping this solution as the working solution given by:

$$Pr = \prod_{i=1}^{Q} \exp\left\{-\frac{F_i(\mathbf{s0f},\mathbf{g1}) - F_i(\mathbf{s0f},\mathbf{g0})}{T_i}\right\} \tag{19}$$

where Q refers to the number of objective functions and F refers to an objective function [19]. The algorithm continues to iterate in this inner loop for a user defined number of iterations (m) known as the length of a Markov chain (using counter im). At the end of each Markov chain, each temperature is then reduced by a user-defined factor which decreases the likelihood of accepting higher value objective functions solutions [21]. At this point an "intelligent return to base" strategy, proposed by Suppapitnarm et al. [19], is employed to explore the solutions at the extreme ends of the pareto-optimal set. More specifically, the degree of isolation I of each solution is calculated by:

$$I(\mathbf{gj}) = \sum_{k=1}^{As} \sum_{i=1}^{Q} \left\{ \frac{F_{i(\mathbf{gj})} - F_{i(\mathbf{gk})}}{F_{imax} - F_{imin}} \right\}^2 \tag{20}$$

where **gj** refers to the jth pareto-optimal solution, As is the total number of pareto-optimal solutions at the particular point in the algorithm, and F_{imax} and F_{imin} are the maximum and minimum values, respectively, of the ith objective function. The pareto-optimal solutions are then listed in order of decreasing value of isolation. At the first intelligent return to base, any of the As pareto-optimal solutions are selected as the working solution. At each later return to base, the algorithm selects from only the top ψAs solutions, where ψ reduces by a value of 0.9 each time. Therefore, as the algorithm progresses, at each return to base, only the more and more isolated solutions are selected. ψAs has a prescribed lower limit (two for this research) [19]. This intelligent return to base strategy enables the algorithm to explore the extreme edges of the pareto-optimal set. Note that Suppapitnarm et al. [19] propose a different strategy for when the return to base strategy is implemented which increases with intensity as the algorithm progress [19]. However, this research simplified this to just return to base at the end of each Markov chain and found excellent results. This outer loop is performed for a user defined number of times (n) for which there has been no update to the pareto-optimal set (using the counter in). The final result of this procedure is a pareto-optimal set of solutions from which the engineer can choose.

The sizing optimization in this research was implemented using the DLS algorithm (Fig. 4, dashed lines). This algorithm is another iterative improvement algorithm like SA without the capability of accepting higher weight solutions (see ex. [26]). As the shape optimization procedure iterates through different geometries, for each geometry (denoted $\mathbf{g}^*$) sizing optimization is performed for minimum self-weight. The DLS algorithm begins by selecting an initial, feasible solution (**s0**) from a database of steel, API line pipe section sizes which are ordered by increasing cross-sectional area [14]. A feasible solution is one in which all members meet the section profile constraints throughout opening (S_S is the set of all feasible solutions). This version of the DLS algorithm initially selects the solution with the largest area for each member. Both objective functions are evaluated. DLS finds a new solution (**s1**) by perturbing the variables in (**s0**) along the database of sections sizes. If the self-weight of the new solution ($W(\mathbf{s1}, \mathbf{g}^*)$) is less than that of the current solution ($W(\mathbf{s0}, \mathbf{g}^*)$), then **s1** becomes the new working solution. Otherwise, **s0** remains the working solution upon which the algorithm iterates. The algorithm continues to iterate until convergence which is defined as a certain number of iterations in which the value of the weight has not decreased. The final solution (**s0f**) is the last working solution when the algorithm has converged.

For both algorithms, certain parameters need to be selected by the user. For the MOSA algorithm this includes the number of design variables to be varied at each perturbation (v), the amount of perturbation permitted along the database of variables (pm), the factor by which the temperature is reduced at the end of each Markov chain (r), the length of the Markov chain (m), and the number of Markov chains until convergence (n). The authors determined the best values for each of these parameters by performing single-objective optimization for each objective function using a variety of combinations of parameters. Ten numerical tests were performed for each combination. The most robust combination – meaning the combination with the lowest average value for each objective function and the lowest standard deviation – was selected. Table 1 lists the final selection of parameters for each form. The reader is referred to Thrall (2011) for details of these studies. For DLS, the parameters include v, pm, and the number of iterations until convergence (it). The values of these parameters were chosen based on a survey of numerical tests for a variety of combinations (using a selected set of geometric design variables). The most robust combination was selected. The reader is referred to Table 2 for the DLS parameters used for each form and to Thrall (2011) for details of the numerical tests performed for this selection.

Table 1
Parameters for MOSA Shape Optimization. The left column provides the name of the form. The other columns indicate the parameters employed including the number of variables to be varied (v), the amount of perturbation permitted (pm), the length of the Markov chain (m), and the number of Markov chains to convergence (n).

Form	v	pm	r	m	n
Back-stay bascule	1	10	0.9	200	2
Piston bascule	1	5	0.9	200	2
Main-span operating rope bascule	1	15	0.9	200	2

3. Three novel linkage-based forms

This research presents three linkage-based forms which were developed using this design methodology and optimization procedure. Each form was designed for the Woodrow Wilson Bridge Replacement Design Competition (1998) site and meets its requirements related to clearance, width, and loading [11]. Each is of the double-leaf bascule configuration, where the term bascule here refers to any movable bridge that rotates about a horizontal axis [2]. The site requires a 21 m vertical clearance when closed and a 41 m vertical clearance when open over a 53 m wide navigational channel [11]. To meet these clearance requirements, each leaf has a span of 38 m and opens to an angle β of 60 degrees. For all three designs, a 24 m wide deck (to allow for six, 3.7 m wide lanes) based on the section properties of an existing movable bridge is assumed. As prescribed by the design competition, the design method is LRFD [11].

3.1. Back-stay bascule design

The design for the first form – the back-stay bascule design – has been discussed throughout the paper. The left column of Fig. 5 shows an idealized diagram of the design in the closed and open configurations. The structural optimization procedure described in the previous section was employed to determine the geometry and the section profiles of the final design as shown in the right column of Fig. 5. The design variables and constraints for both shape and sizing optimization are given in the following two paragraphs.

The geometric design variables include the initial positions of points A, B, D, and E relative to point F which were allowed to vary between 0 and 76 m in 0.3 m increments. The geometric constraints include (1) the horizontal coordinate of pin support A must be greater than that of pin support B ($X_B > X_A$), (2) the vertical coordinate of point E must be positive at all times to prevent the system from dipping below the deck ($Y_E > 0$), (3) the horizontal coordinate of point G must be greater than that of point D

Table 2
Parameters for DLS sizing optimization. The left column provides the name of the form. The other columns indicate the parameters employed including the number of variables to be varied (v), the amount of perturbation permitted (pm), and the number of iterations to convergence (it).

Form	v	pm	it
Back-stay bascule	1	15	500
Piston bascule	1	15	100
Main-span operating rope bascule	1	15	100

($X_G > X_D$) to ensure that member AD does not cross the deck, (4) the initial horizontal coordinate of point E is less than that of point D ($X_{Eo} < X_{Do}$) so that the system begins with member AD and member BE crossing and (5) members AD and BE must cross at all stages of opening. With these five geometric constraints, the system is sufficiently constrained to maintain the conceptual design.

The sizing optimization design variables include the sections for members AD, BE, ED, and rope DG. Members AD, BE, and ED are selected from a database of API line pipe [14]. The sizing optimization constraints require that members AB, BE, and ED meet design code at all positions. Rope DG is comprised of a number of stay cable strands (each assumed to have a standard cross-sectional area of 140 mm^2). The optimization process selects the number of strands for this cable (and therefore the total cross-sectional area of the member) ranging anywhere between 1 and a maximum of 91 strands. The capacity of rope DG is defined as $\phi P_n = \phi \sigma A$ where the resistance factor ϕ is assumed to be .65, the grade σ is assumed to be 1862 MPa (as given by industry standards [27]), and the area A is defined through the sizing optimization process. The force under factored load combinations of the cable DG must always be less than ϕP_n. This rope is required to stay in tension throughout opening. The section properties of the operating rope (member EF) are not a design variable. To be used with a conventional gear driven mechanical system, 6×19 fiber core rope with filler wire was selected. Six wire ropes were chosen to maximize capacity while also considering feasibility concerns related to wrapping multiple wires around a mechanical system simultaneously. In preliminary studies of this conceptual design, the force in this member controlled the feasibility of designs and six of the largest 6×19 fiber core rope with filler wire were required to find an initial working design. Rather than waste computational time on designing the rope (which would ultimately be chosen as the largest one available), the largest diameter (57.2 mm) was prescribed for each of the six ropes [28]. This rope is also required to stay in tension. The live load rope would be included in a final design, but was not considered during the optimization process.

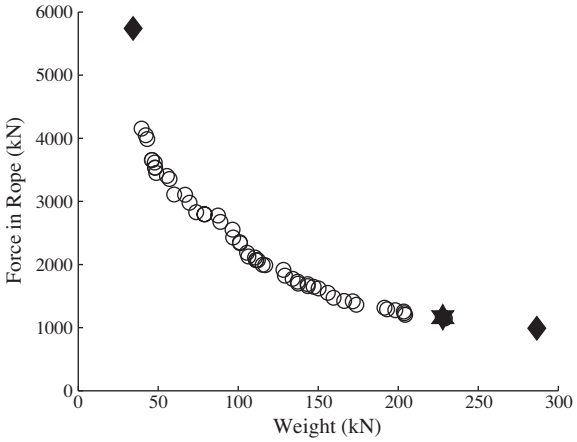

Fig. 6. Pareto-optimal solutions at convergence. The circles represent the pareto-optimal solutions found by the algorithm, the diamonds are the best results from each single-objective optimization process, and the star shows the point selected as the final solution.

The result of multi-objective optimization is a pareto-optimal set of solutions from which an engineer can choose based on design priorities. Fig. 6 shows the pareto-optimal set of solutions at convergence as circles. Prior to employing multi-objective optimization, single-objective optimization for minimum self-weight and for minimum force in the operating member were performed. The best results of this process are shown as diamonds in Fig. 6 as reference points. Notice that the pareto-optimal set spans between the two extreme solutions found through single-objective optimization. From this set, the engineer must select a final design. For this case study, the final design was chosen based on the capacity of the operating rope (member EF). The capacity was determined based on AASHTO LRFD movable bridge design code and the nominal strength of 6×19 fiber core wire ropes [28]. The pareto-optimal point with a force below this capacity but with the least self-weight was chosen (star in Fig. 6). Table 3 provides the

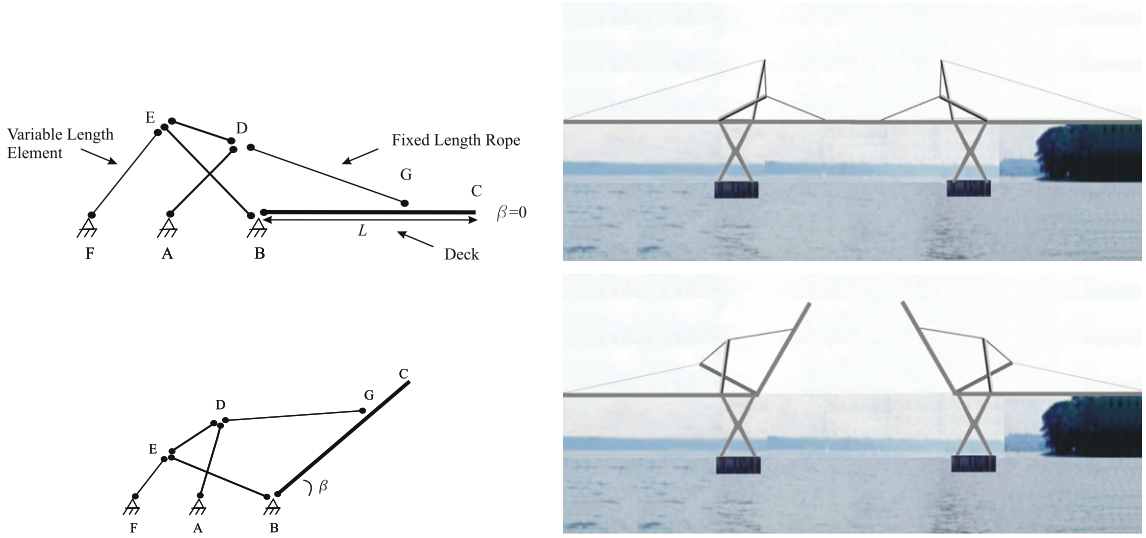

Fig. 5. Design concept (left column) and final rendering (right column) of the back-stay bascule design in the closed (top row) and open (bottom row) positions.

self-weight of the main structural elements (members AD, EB, and ED) and the maximum force in the operating rope (member EF) throughout opening. The right column of Fig. 5 shows a rendering of this final design. The pin supports at points A and B are supported by an X-shaped pier. The pin support at point F is attached to the fixed length span.

3.2. Piston bascule design

The design concept for a second four-bar linkage form – the piston bascule design – is shown in Fig. 7 in the closed and open positions. Here, the four-bar linkage is comprised of members ED, DC, the deck (member BC), and the fixed length between pin supports E and B. DG is a variable length member which expands to lift the deck. Since this member is always in compression, it would need to be a piston (shown as a black rectangle in Fig. 7). Note that member ED is not connected to the deck. Pin connections are indicated as filled circles.

Shape and sizing optimization were performed to determine the geometry and the section profiles of the system. The shape optimization design variables include the initial positions of points E, G, and D relative to point B which are permitted to range between 0 and 38 m in 0.3 m increments. The reader is referred to Thrall (2011) for the parametric model, kinematic equations, and geometric constraints for this problem. The sizing optimization design variables are the sections for members ED, DC, and DG which are selected from a database of API line pipe [14]. For the purpose of this study, it is assumed that the piston (member DG) is a telescoping member with the properties of an API line pipe section. Custom-built pistons, like those in the Temse and Tervate Bridges, could be employed to provide the necessary capacity and stroke length [8,9].

Fig. 7 shows a rendering of the final design selected. Notice that a back-stay has been added to mirror member ED in the closed position. This was added in the rendering with the intent of reducing the bending moment that would result in the pier supporting pin supports B and E. Additional analysis would be required to determine the appropriate section sizes of the pier and this back-stay. Table 3 summarizes the self-weight of the main structural elements (members ED, DC, and DG) and the maximum force in the piston as the bridge moves.

3.3. Main-span operating rope design

A third form – the main-span operating rope design – is shown as a diagram in the open and closed positions in the left column of Fig. 8. Here, members ED, DB, the deck (member AC), and the fixed distance between pin supports A and E comprise the four-bar linkage. The operating member (member AD) is a variable length element, which, when shortened, lifts the deck. This member was assumed to be an operating rope with a conventional gear driven mechanical system at pin support A. As a result, a constraint that required that this member remain in tension was included. Alternatively, this constraint could have been released and a piston could have been considered. Like the back-stay bascule design, a live load rope (connecting pin support A to node D) would be required to carry the live load of the bridge when closed but becomes slack as the variable length element shortens. This live load rope was not considered during the optimization process, but would need to be included in a final design. Note that there is no connection between member ED and the deck. Pin connections are indicated as filled circles.

Shape and sizing optimization were once again performed to determine the geometry and the section profiles of the system. Shape optimization design variables included the initial positions of points E, D, and B relative to point A which were permitted to range between 0 and 38 m in 0.3 m increments. The sizing optimization variables included the section profiles of members ED and DB which were selected from a database of API line pipe. As in the case of the back-stay bascule design, the operating rope was assumed to be comprised of six, 6×19 fiber core rope with filler wire of 57.2 mm diameter. The reader is referred to Thrall (2011) for details of the parametric model, kinematic equations, and geometric constraints.

The right column of Fig. 8 shows the final rendering of the design. An X-shaped pier supports pin supports A and E. Table 3 summarizes the self-weight of members ED and DB and the maximum force in the operating rope throughout opening.

Table 3
Comparison of forms. The left column provides the name of the form, the middle column provides the self-weight of the linkage elements for that form, and the right column provides the maximum force in the operating member throughout opening. Each form fulfills the same structural criteria and boundary conditions, but employ linkages in different configurations.

Form	Self-weight (kN)	Force (kN)
Back-stay bascule	228	1166
Piston bascule	88	2551
Main-span operating rope bascule	103	2844

4. Discussion

Final designs for each concept were selected from the pareto-optimal set of solutions. Based on this final selection, the piston bascule design has the lowest self-weight and the back-stay bascule has the lowest maximum axial force for operation (Table 3). Since these linkage-based movable bridges are new forms, it is difficult to accurately compare their performance against traditional bascule bridges. The most appropriate comparison is a Strauss heel trunnion bascule, such as the 66 m bascule span of the Florida East Coast Railway's Bridge over the St. Johns River at Jacksonville (completed in 1925). Though it carries two railroad tracks as opposed to six vehicular lanes and has a longer span than the forms presented here, it provides a reference for comparison. The counterweight truss represents the aspect of a heel trunnion bridge most closely related to the linkage elements for the forms presented here (for which self-weights are given in Table 3). Based on the available section properties and geometry, the self-weight of one plane of the counterweight truss was calculated to be approximately 811 kN [29]. This is more than three and a half times the self-weight of the heaviest of the linkages of the three forms presented here. This comparison highlights a potential advantage of these new linkage-based forms as compared to the only comparable existing form.

The self-weight and force for operation (Table 3) indicate the advantages and disadvantages of each of the three forms compared against one another. However, other factors also need to be considered when evaluating each form. One critical choice for a designer to consider is the operating system. In this research, the operating system was pre-selected by the designer prior to the optimization process, and as a result certain constraints needed to be incorporated. For example, an operating rope with a conventional gear driven mechanical system requires that the rope always be in tension. This was implemented in the optimization process as a constraint on the variable length element for both the back-stay bascule and main-span operating rope bascule forms. Alternatively, a piston could operate in tension or compression and therefore this constraint could be released for forms such as the piston bascule design. Such constraints have the potential to significantly influence the shape optimization process. Another influencing

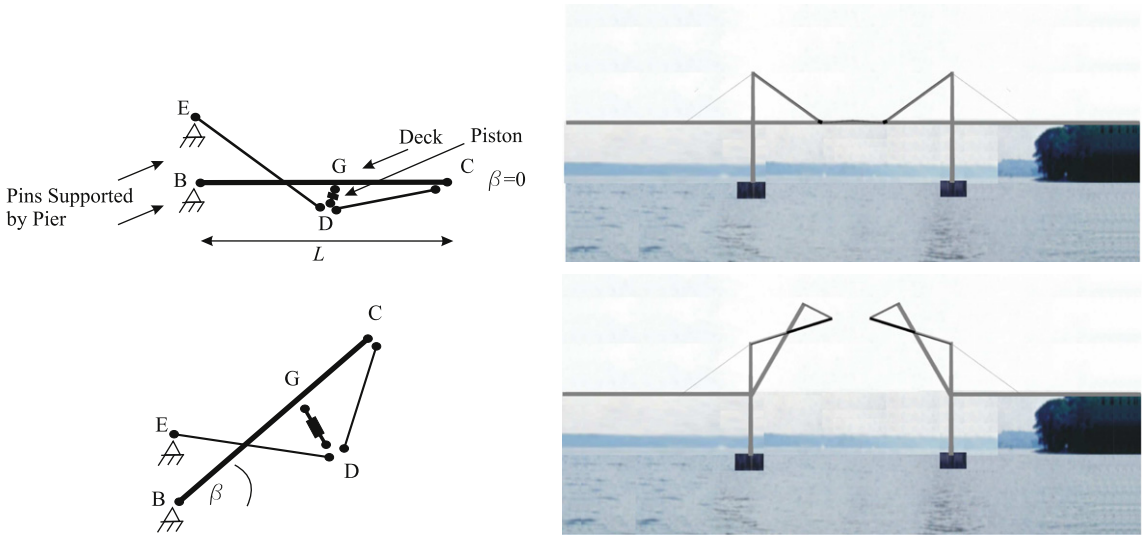

Fig. 7. Design concept (left column) and final rendering (right column) of the piston bascule design in the closed (top row) and open (bottom row) positions.

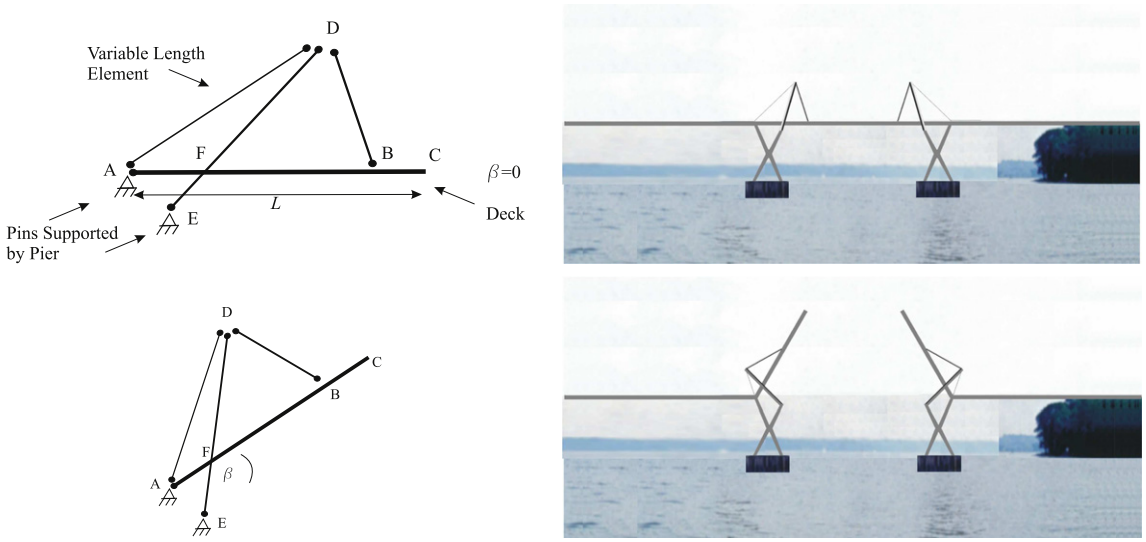

Fig. 8. Design concept (left column) and final rendering (right column) of the main-span operating rope bascule design in the closed (top row) and open (bottom row) positions.

factor related to the choice of operating system, which was not incorporated into the optimization process in this research, is the total change in length of the operating member. A design in which the variable length member undergoes a large change in length would favor an operating rope, while a piston could be employed for smaller change in length geometries. In addition to considering the type of operating system, it is also crucial to consider its location related to convenience of installation and maintenance as well as safety from vessel collision. For example, both the back-stay bascule and the main-span operating rope bascule designs offer an advantage since the operating system for each is above deck level on the fixed span thereby making it easily accessible. Alternatively, the piston bascule's operating piston is below deck level and is over the navigational channel, therefore increasing the difficulty of maintenance and making the piston more susceptible to vessel collision.

This research was primarily interested in finding optimized forms for minimum self-weight and minimum force for operation. However, for a final design, additional analysis and design is necessary, including (1) analysis under additional loading conditions (including but not limited to dynamic, fatigue, alternative wind, earthquake, and point live loads), (2) deck design, (3) analysis of the operating mechanism, (4) consideration of the erection procedure, (5) foundation design, (6) design of joints (including the effects of friction and eccentricity), and (7) determination of appropriate maintenance programs. All designs were considered from a two-dimensional perspective only for the purpose of finding planar forms. A final design would need to also incorporate lateral bracing and the effects of lateral loads such as wind. Thus far, all three designs are non-counterbalanced. To further reduce the force required for operation, the designer could consider adding counterweights on the backspan of each of the movable spans.

5. Conclusion

This paper presented a design methodology and three novel forms for linkage-based movable bridges. The design methodology,

which included physical shape-finding, generating a parametric model and kinematic equations, and multi-objective structural optimization, resulted in three innovative conceptual designs with corresponding sets of pareto-optimal solutions that balanced self-weight with force for operation. To the best of the authors' knowledge, this is the first exploration of linkage-based movable bridges, aside from those few examples discussed in the introduction.

This paper suggests the beginning of an exploration of linkages for movable bridge design. The three novel forms presented here demonstrate the potential of employing four-bar linkages for bascule-type movable bridge forms. Additional opportunities for exploring linkage-based movable bridge forms include (1) investigating alternative types of linkages and (2) exploring the application of linkages for swing or vertical lift type motion. This area of research appears to be rich in opportunities for designing alternative forms for movable bridge forms using linkages.

Acknowledgements

This material is based upon work supported by the National Science Foundation Graduate Research Fellowship under Grant No. DGE-0646086. Dr. Thrall is also grateful for support from the Norman J. Sollenberger Fellowship. Dr. Paya-Zaforteza has been involved with this research project while on appointment as a Postdoctoral Fellow under the Program for Postdoctoral Stays administered by the Spanish Ministry of Education (Contract Number EX-2008-0669). The authors are grateful for the advice of Professors Maria E.M. Garlock (Princeton University), David P. Billington (Princeton University), and James K. Guest (Johns Hopkins University). The authors would also like to thank the anonymous reviewers for their helpful comments and suggestions.

References

[1] Wallner M, Pircher M. Kinematics of movable bridges. J Bridge Eng 2007;12(2):147–53.
[2] Koglin TL. Movable bridge engineering. Hoboken, NJ: John Wily & Sons, Inc.; 2003.
[3] Hartenberg RS, Denavit J. Kinematic synthesis of linkages. New York, NY: McGraw-Hill Book Company; 1964.
[4] Gantes CJ. Deployable structures: analysis and design. Boston, MA: WIT Press; 2001.
[5] Piñero EP. Expandable space framing. Progress Archit 1962;43(6):154–5.
[6] Euler L. Mechanica, sive, Motus scientia analytice exposita. St. Petersburg, Russia: Petropoli: Ex typographia Academiae Scientiarum; 1736.
[7] Waddell JAL. Bridge engineering. New York, NY: John Wily & Sons, Inc.; 1916.
[8] Ney L, Adriaenssens S. The piston-stayed bridge: a novel typology for a mobile bridge at Tervate, Belgium. Struct Eng Int 2007;17(4):302–5.
[9] Adriaenssens S, Ney L, Mallie M. Piston stayed bascule bridge: a novel mobile bridge typology at Temse, Belgium, 2008. In: International association for bridge and structural engineering congress: creating and renewing urban structures, September 17–19. Chicago, IL, USA.
[10] Schlaich J, Bergermann R, Bogle A, Cachola Schmal P, Flagge I. Leicht Weit = light structures: Jorg Schliach, Rudolf Bergermann. New York, NY: Prestel; 2003.
[11] Anon. Selection panel review workbook: Woodrow Wilson Bridge Design Competition, 1998. Courtesy of the Princeton University Maillart Archive.
[12] K'NEX Brands LP. K'nex. Retrieved February 18, 2011, from: http://www.knex.com, 2011.
[13] Thrall AP. Design and optimization of linkage-based movable bridge forms, Ph.D. dissertation. Princeton, NJ: Princeton University; 2011.
[14] WOODCO. Carbon steel pipe dimensions and weights. Retrieved December 27, 2010, from: http://www.woodcousa.com/pipe_schedule.htm, 2006.
[15] AASHTO. American Association of State Highway and Transportation Officials (AASHTO) Load and Resistance Factor Design (LRFD) Bridge Design Specifications: Customary US Units. 4th ed. Washington, DC: AASHTO; 2007.
[16] AASHTO. AASHTO LRFD movable highway bridge design specifications. 2nd ed. Washington, DC: AASHTO; 2007.
[17] Thrall AP. Shape-finding of a deployable structure using simulated annealing. J Int Assoc Shells Spatial Struct 2011;52(4):241–7.
[18] Kirkpatrick S, Gelatt Jr CD, Vecchi MP. Optimization by simulated annealing. Science 1983;220(4598):671–80.
[19] Suppapitnarm A, Seffen KA, Parks GT, Clarkson PJ. Simulated annealing algorithm for multiobjective optimization. Eng Optim 2000;33(1):59–85.
[20] Yepes V, Alcala J, Perea C, Gonzalez-Vidosa F. A parametric study of optimum earth-retaining walls by simulated annealing. Eng Struct 2008;30(3):821–30.
[21] Paya I, Yepes V, Gonzalez-Vidosa F, Hospitaler A. Multiojbective optimization of concrete frames by simulated annealing. Computer-Aided Civil Infrast Eng 2008;23(8):596–610.
[22] Ohsaki M, Tagawa H, Pan P. Shape optimization of reduced beam section under cyclic loads. J Const Steel Res 2009;65(7):1511–9.
[23] Paya-Zaforteza I, Yepes V, Hospitaler A, Gonzalez-Vidosa F. CO2-optimization of reinforced concrete frames by simulated annealing. Eng Struct 2009;31(7):1501–8.
[24] Leng J, Guest JK, Schafer BW. Shape optimization of cold-formed steel columns; in review.
[25] Medina JR. Estimation of incident and reflected waves using simulated annealing. J Waterway Port Coastal Ocean Eng 2001;127(4):213–21.
[26] Perea C, Alcala J, Yepes V, Gonzalez-Vidosa F, Hospitaler A. Design of reinforced concrete bridge frames by heuristic optimization. Adv Eng Softw 2010;39(8):676–88.
[27] Tensacciai. Stay cables. Retrieved February 24, 2011, from: http://www.tensacciai.it/uploads/File/cata/StayCable2009.pdf, 2009.
[28] Southwest Wire Rope LP. Wire rope. Retrieved March 5, 2011, from: http://www.swwrinc.com/pdf/cp05.pdf, 2011.
[29] Wall E. Florida east coast railway's strauss trunnion bascule bridge over the St. Johns River at Jacksonville. Retrieved October 26, 2011, from: http://users.ipa.net/ewall/fecbr.htm, 1997.